Probing the importance of hydrogen bonds in the active site of the subtilisin nattokinase by site-directed mutagenesis and molecular dynamics simulation

Zhong-liang ZHENG*, Mao-qing YE*, Zhen-yu ZUO*, Zhi-gang LIU*, Keng-chang TAI† and Guo-lin ZOU*[1]

*National Key Laboratory of Virology, Life Sciences College, Wuhan University, Wuhan 430072, China, and †Department of Life Sciences, National Tsing Hua University, Hsinchu 30043, Taiwan

Hydrogen bonds occurring in the catalytic triad (Asp^{32}, His^{64} and Ser^{221}) and the oxyanion hole (Asn^{155}) are very important to the catalysis of peptide bond hydrolysis by serine proteases. For the subtilisin NK (nattokinase), a bacterial serine protease, construction and analysis of a three-dimensional structural model suggested that several hydrogen bonds formed by four residues function to stabilize the transition state of the hydrolysis reaction. These four residues are Ser^{33}, Asp^{60}, Ser^{62} and Thr^{220}. In order to remove the effect of these hydrogen bonds, four mutants ($Ser^{33} \rightarrow Ala^{33}$, $Asp^{60} \rightarrow Ala^{60}$, $Ser^{62} \rightarrow Ala^{62}$, and $Thr^{220} \rightarrow Ala^{220}$) were constructed by site-directed mutagenesis. The results of enzyme kinetics indicated that removal of these hydrogen bonds increases the free-energy of the transition state ($\Delta\Delta G_T$). We concluded that these hydrogen bonds are more important for catalysis than for binding the substrate, because removal of these bonds mainly affects the k_{cat} but not the K_m values. A substrate, SUB1 (succinyl-Ala-Ala-Pro-Phe-*p*-nitroanilide), was used during enzyme kinetics experiments. In the present study we have also shown the results of FEP (free-energy perturbation) calculations with regard to the binding and catalysis reactions for these mutant subtilisins. The calculated difference in FEP also suggested that these four residues are more important for catalysis than binding of the substrate, and the simulated values compared well with the experimental values from enzyme kinetics. The results of MD (molecular dynamics) simulations further demonstrated that removal of these hydrogen bonds partially releases Asp^{32}, His^{64} and Asn^{155} so that the stability of the transition state decreases. Another substrate, SUB2 (H-D-Val-Leu-Lys-*p*-nitroanilide), was used for FEP calculations and MD simulations.

Key words: catalytic mechanism, enzyme kinetics, hydrogen bond, molecular dynamics simulation, site-directed mutagenesis, subtilisin NAT.

INTRODUCTION

NK (nattokinase) is a potent fibrinolytic enzyme from *Bacillus natto* [1]. Functionally similar to plasminogen on the basis of substrate specificity, NK dissolves fibrin directly. In addition, it also enhances the body's production of both plasmin and other clot-dissolving agents, including urokinase. In some aspects, NK is actually superior to conventional clot-dissolving drugs [2], which have many benefits including convenient oral administration, known efficacy, prolonged effects, cost effectiveness and prevention of clot formation. NK has been demonstrated to have pH and temperature stability and so can be found in the gastrointestinal tract [3].

As a member of the subtilisin family of serine proteases, NK has the same conserved catalytic triad (Asp^{32}, His^{64} and Ser^{221}) and oxyanion hole (Asn^{155}) [4]. The serine protease subtilisin is an important industrial enzyme, as well as a model for understanding the relationship between enzyme structure and function [5]. Subtilisin has many advantages, such as rapid gene sequencing and cloning, widespread expression, ease of purification and the availability of abundant crystal structures. For these reasons, subtilisin became a model system for protein engineering studies in the 1980s. Twenty years later, mutations in well over 50 % of the 275 amino acids in subtilisin have been reported in the scientific literature. Most subtilisin molecular engineering has involved the catalytic amino acids, substrate-binding regions and investigation of stabilizing mutations [6]. Temperature and pH stability is the property of subtilisin that is most amenable to enhancement, yet perhaps the least well understood.

Wells and Carter [7] have reported on the catalytic mechanism of subtilisin. A large body of literature indicates that these enzymes catalyse reactions by binding the substrate in the transition state more tightly than the reactants or products [8]. Enzymes often accomplish this using weak binding forces such as hydrogen bonds, electrostatic and hydrophobic interactions [9]. Based on the Wells and Carter [7] mechanism, we aimed to determine the relationship between structure and function in NK. In order to investigate the importance of hydrogen bonds in the catalytic triad and oxyanion hole of NK, the four residues Ser^{33}, Asp^{60}, Ser^{62} and Thr^{220} were chosen and each mutated into alanine. Both enzyme kinetics and FEP (free-energy perturbation) calculations were used to evaluate the catalytic function of these four residues in NK. MD (molecular dynamics) simulations were used to further investigate how these four residues affected the stability of the transition state of NK.

MATERIALS AND METHODS

Materials

Bacillus subtilis var. *natto* strain AS 1.107 was purchased from the Institute of Microbiology, Chinese Academy of Sciences (Beijing, China). *Escherichia coli* BL21(DE3) and the vector pET-28a were from Novagen. Bovine fibrinogen, thrombin and

Abbreviations used: E, enzyme; S, substrate; E–S, enzyme–substrate non-covalent complex; ETS, enzyme-transition state complex; FEP, free-energy perturbation; MD, molecular dynamics; NK, nattokinase; SUB1, substrate 1 (succinyl-Ala-Ala-Pro-Phe-*p*-nitroanilide); SUB2, substrate 2 (*H*-D-Val-Leu-Lys-*p*-nitroanilide).

[1] To whom correspondence should be addressed (email zouguolin@whu.edu.cn).

Table 1 Synthetic oligonucleotides used for site-directed mutagenesis

Underlined sequences denote the sites indicated; mut, mutated.

Subsitution	Oligonucleotide sequences
Wild-type	Forward: 5′-TGTGGATCCGCGCAATCTGTTCCTTATGGC-3′, BamHI site
	Reverse: 5′-CTGGAGCTCTTGTGCAGCTGCTTGTACGTT-3′, SacI site
Mutant	
S33A	Forward: 5′-CGTAAAAGTAGCTGTTATCGACGCAGGAATTGACTCTTCTCATCC-3′, mut site
	Reverse: 5′-GGATGAGAAGAGTCAATTCCTGCGTCGATAACAGCTACTTTTACG-3′, mut site
D60A	Forward: 5′-GAAACAAACCCATACCAGGCAGGCAGTTCTCACGGTA-3′, mut site
	Reverse: 5′-TACCGTGAGAACTGCCTGCCTGGTATGGGTTTGTTTC-3′, mut site
S62A	Forward: 5′-CCATACCAGGACGGCGCTTCTCACGGTACGCAT-3′, mut site
	Reverse: 5′-GGTATGGTCCTGCCGCGAAGAGTGCCATGCGTA-3′, mut site
T220A	Forward: 5′-CGGCGCTTATAACGGAGCATCCATGGCGACTCC-3′, mut site
	Reverse: 5′-GGAGTCGCCATGGATGCTCCGTTATAAGCGCCG-3′, mut site

urokinase were purchased from Sigma (St. Louis, MO, U.S.A.). SUB1 (substrate 1; succinyl-Ala-Ala-Pro-Phe-*p*-nitroanilide) was purchased from Sigma. Ampicillin and kanamycin were from Takara (Dalian, China). Restriction enzymes and DNA-modifying enzymes were purchased from Promega. Sephadex G-200 was purchased from Pharmacia Biotech (Uppsala, Sweden).

Construction and purification of NK mutants

B. subtilus var. *natto* was used as the source of genomic DNA. *E. coli* BL21 (DE3) was the host bacterial strain for the pET-28a vector expression system. The NK mature peptide gene [$aprN_{(MP)}$] was cloned into the plasmid pET-28a, and each of the four mutations ($Ser^{33} \rightarrow Ala^{33}$, $Asp^{60} \rightarrow Ala^{60}$, $Ser^{62} \rightarrow Ala^{62}$, and $Thr^{220} \rightarrow Ala^{220}$) was introduced into the $aprN_{(MP)}$ gene by sited-directed mutagenesis. Mutagenesis was performed by the overlap extension method [10,11]. As shown in Table 1, oligonucleotide sequences for the wild-type NK were used for PCR. Restriction enzymes BamHI and SacI were used to modify the $aprN_{(MP)}$ gene and pET-28a. The mutant phagemids were verified by dideoxy-mediated sequencing [12,13]. Subtilisin mutants were cultured at 37 °C in Luria–Bertani medium and purified on a Sephadex G-200 column as described by Zhang et al. [14].

Assay of enzyme activity and kinetic studies

Quantitative analysis of fibrinolytic activity was conducted by the standard fibrin plate method [15].

Kinetic parameters were assayed with the substrate SUB1 in 1 ml of 100 mM Tris/HCl (pH 8.60), 4 % (v/v) DMSO at (25 ± 0.2) °C as described by Carter and Wells [7]. Enzyme concentrations were determined spectrophotometrically at 280 nm. Subtilisin mutants were assayed at concentrations of about 5 nM for the most active mutants and 1 μM for the least active mutants. Initial rates of hydrolysis were measured at substrate concentrations in the range 0.2–5 × K_m.

MD simulations and FEP calculations

A refined three-dimensional model of NK was constructed by the method of Zheng et al. [16]. Based on this model, the simulated mutations ($Ser^{33} \rightarrow Ala^{33}$, $Asp^{60} \rightarrow Ala^{60}$, $Ser^{62} \rightarrow Ala^{62}$, and $Thr^{220} \rightarrow Ala^{220}$) were performed by the TRITON program [17,18]. Three simulations of MD were carried out: (i) on the enzyme itself (E), (ii) on the enzyme–substrate noncovalent complex (E–S), and (iii) on the model of the enzyme-transition state complex (ETS) for acylation catalysis by the serine protease (Figure 1). In each case, we began with the

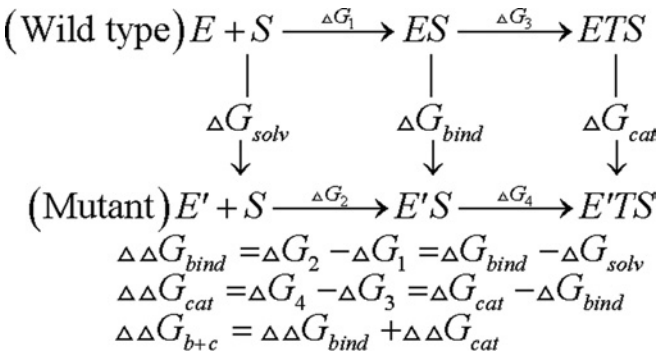

Figure 1 Thermodynamic cycle for substrate binding and catalysis

three-dimensional model of NK. For the E–S, we docked SUB2 (substrate 2; *H*-D-Val-Leu-Lys-*p*-nitroanilide) with neutral N- and C-terminal residues into the active site of NK and orientated it so that its scissile bond was in position to be attacked by Ser^{221}. For the ETS, we used a structure in which His^{64} was protonated and the O_γ of Ser^{221} formed a covalent bond with the carbonyl carbon of the substrate, which was sp^3 hybridized.

In all three modelled structures E, E–S and ETS, WATBOX216 waters were added to the system to fill the space within 18 Å (1 Å = 0.1 nm) of the O_γ (Ser^{221}) in the XLEaP module of AMBER7 [2]. The system energy was minimized with a harmonic constraint of 100 kJ/mol per Å^2 for 5000 steps, including 2500 steps of steepest descent, followed by 2500 steps of conjugated gradient. After that, the system was equilibrated using MD at constant temperature (300 K) and pressure with SHAKE [19] for 50 ps. A constraint of 5 kJ/mol per Å^2 was used. Next, the free-energy calculations were initiated and continued for 100 ps. In all of the theoretical simulations, an 8 Å nonbonded cutoff was used. A PARM99 force field was used for the enzyme and a GAFF force field was used for the ligand.

The free-energy simulations using the GIBBS module of the AMBER program were carried out on these systems using the method of dynamically modified windows [20]. The free-energies for the forward ($\lambda = 1 \rightarrow 0$) direction were obtained in each system. In all calculations, a duration of 40 ps was used for this simulation with timed steps of 0.002 fs. The nonbonded cutoff was 15 Å.

RESULTS AND DISCUSSION

Mutant design and preparation

Based on the three-dimensional structure of NK [16], the hydrogen bonds in the active centre of NK are discussed below. As shown in Table 2, there are 16 important hydrogen bonds interacting with the catalytic triad (Asp^{32}, His^{64} and Ser^{221}) and the oxyanion hole (Asn^{155}). Four hydrogen bonds, including hydrogen bond-1, hydrogen bond-4, hydrogen bond-13 and hydrogen bond-14, are formed between the HN atom and the O atom, which are both backbone atoms. Since these four hydrogen bonds are not altered by the site-directed mutagenesis of the catalytic residues, we have disregarded these four hydrogen bonds. The other 12 hydrogen bonds are more important because they are formed not only between backbone atoms and residue atoms but also between residue atoms. It is evident that the mutation of any of these residues will disrupt the hydrogen bonds.

We further determined that four residues have an important function for the stability of the NK active site. These four residues are Ser^{33}, Asp^{60}, Ser^{62} and Thr^{220}. As shown in Figure 2, the loop

Table 2 Hydrogen bonds around the catalytic triad (Asp^{32}, His^{64} and Ser^{221}) and oxyanion hole (Asn^{155}) of NK

These hydrogen bonds were determined using DeepView 3.7.; bond length was determined by MD simulation.

	Proton-supplying group		Proton-accepting group		
H-bonds	Residue	Atom	Residue	Atom	Bond length (Å)
1	Asp^{32}	HN	Val^{93}	O	2.2 ± 0.2
2	Ser^{33}	HN	Asp^{32}	$O_{\delta}1$	1.8 ± 0.1
3	Ser^{33}	HO_{γ}	Asp^{60}	$O_{\delta}1$	1.7 ± 0.1
4	Gly^{61}	HN	Ser^{33}	O	2.0 ± 0.3
5	Ser^{62}	HO_{γ}	Ser^{33}	O_{γ}	2.0 ± 0.3
6	Ser^{62}	HN	Asp^{60}	$O_{\delta}1$	2.7 ± 0.7
7	Ser^{63}	HN	Asp^{60}	$O_{\delta}1$	2.7 ± 0.7
8	His^{64}	HNe1	Asp^{32}	$O_{\delta}1$	1.8 ± 0.1
9	His^{64}	HNe1	Asp^{32}	$O_{\delta}2$	2.7 ± 0.5
10	His^{64}	HN	Ser^{62}	O_{γ}	2.3 ± 0.5
11	Thr^{66}	HN	Asp^{60}	$O_{\delta}2$	1.9 ± 0.2
12	Thr^{66}	HO_{γ}	Asp^{60}	$O_{\delta}2$	1.8 ± 0.2
13	Val^{68}	HN	His^{64}	O	2.2 ± 0.3
14	Val^{95}	HN	Asp^{32}	O	2.0 ± 0.2
15	Thr^{220}	HO_{γ}	Asn^{155}	O_{δ}	2.4 ± 0.5
16	Thr^{220}	HN	Asn^{155}	O_{δ}	2.0 ± 0.2

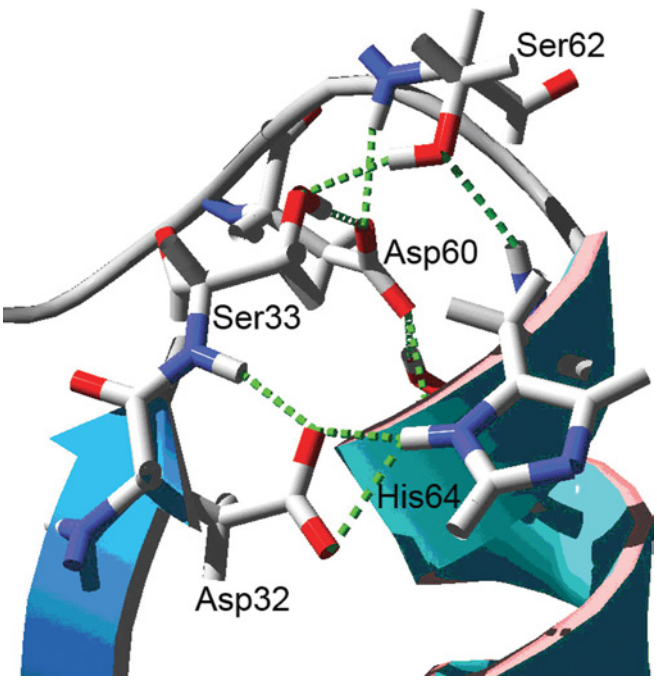

Figure 2 The loop structure of NK including Ser^{33}, Asp^{60} and Ser^{62}

The backbone atoms of NK are indicated by secondary structure colours. Other residues are in conventional scale colours, and labelled by their residue names. This Figure was rendered using DeepView 3.7.

which connects the α-helix and His^{64} is very important. Several hydrogen bonds formed by Ser^{33} link the β-sheet, including Asp^{32}, with the loop. It is obvious that the loop's movement may directly affect the stability of the Asp^{32} and His^{64} residues. The loop includes Asp^{60} and Ser^{62} residues. As shown in Figure 3, the hydrogen bonds formed by the residues Asp^{60} and Ser^{62} play an important role in the stability of the His^{64} residue. The hydrogen bonds formed by Ser^{33} have a great effect on the stability of the Asp^{32} residue. As shown, the removal of these hydrogen bonds will partially release the Asp^{32} and His^{64} backbone atoms so that the Asp^{32} and His^{64} residues can move freely. Therefore we first chose these three residues for site-directed mutagenesis. As demonstrated by Braxton and Wells [21] and Mizushima et al. [22], the Thr^{220} residue can stabilize the transition state in subtilisin BPN′ and we have shown a similar finding for the hydrogen bonds in NK as shown in Figure 3(D). Therefore we examined these hydrogen bonds in NK, to identify the residues that account for stability in NK.

Kinetic analysis and FEP calculations of variant subtilisins

A series of hydrogen bonds were removed by site-directed mutagenesis to investigate the roles of Ser^{33}, Asp^{60}, Ser^{62} and Thr^{220} in enzyme catalysis. Four mutants ($Ser^{33} \rightarrow Ala^{33}$, $Asp^{60} \rightarrow Ala^{60}$, $Ser^{62} \rightarrow Ala^{62}$, and $Thr^{220} \rightarrow Ala^{220}$) were constructed and used for kinetic analysis. In the present study, alanine was used to minimize structural disruption and alternative hydrogen-bonding effects from site-directed mutagenesis. Kinetic analysis was carried out according to the method of Carter and Wells [7]. As shown in Table 3, removal of each of these four residues resulted in a greater reduction (< 3–14-fold) in the k_{cat} value, and a smaller increase (< 3-fold) in the K_m. The effects of this removal on catalytic efficiency were also quantified in terms of the incremental free-energy of transition state stabilization of the mutants compared with the wild-type enyzme. The values are given in Table 3. The $\Delta\Delta G_T$ values of the four mutants are all above 0. Therefore we concluded that the hydrogen bonds formed by the residues Ser^{33}, Asp^{60}, Ser^{62} and Thr^{220} function predominantly in the catalytic step to stabilize the catalytic triad and the oxyanion hole.

By comparison of the NK and subtilisin BPN′ sequences we found the same specificity at the P1 position in NK as in subtilisin BPN′. They both possess the same Gly^{166} at the S1 subsite which is more sensitive to binding phenylalanine than binding lysine or arginine at the P1 position [23]. Moreover, Fujita et al. [24] have proved that SUB1 is more suitable for enzyme kinetics analysis of NK than is SUB2. As a result SUB1 was chosen for enzyme kinetics analysis. However, SUB1 does not display a similar clot-dissolving property with NK [1]. In order to accurately display the mechanism of action of NK, SUB2 was chosen for FEP calculations and MD simulations.

The results of FEP calculations also indicate the function Ser^{33}, Asp^{60}, Ser^{62} and Thr^{220} residues. As shown in Table 3, mutating Ser^{33} into Ala^{33} with water, Michaelis complex or tetrahedral intermediates involves a free-energy change of 7.1 kcal/mol (1 kcal = 4.184 kJ), 7.3506 kcal/mol or 8.7 kcal/mol respectively. This demonstrates that the solvation of the Ala^{33} mutant is unfavoured compared with the native enzyme (containing Ser^{33}) in all three cases; the enzyme itself, the E–S and the tetrahedral intermediate. The mutants $Ser^{62} \rightarrow Ala^{62}$ and $Thr^{220} \rightarrow Ala^{220}$ are similar to the $Ser^{33} \rightarrow Ala^{33}$ mutant, but the $Asp^{60} \rightarrow Ala^{60}$ mutant is different. Mutating Asp^{60} to alanine involves a free-energy change of $-\infty$, this value is variable and does not indicate the advantage gained in mutating Asp^{60} to alanine. Although this result deviates from known enzyme kinetics data, it does suggest the possibility that the solvation of the Ala^{60} mutant is enhanced compared with the native enzyme (containing Asp^{60}) in all three cases. The calculated $\Delta\Delta G_{bind}$ and $\Delta\Delta G_{cat}$ of the $Ser^{33} \rightarrow Ala^{33}$ mutant are 0.3 kcal/mol and 1.3 kcal/mol respectively. The $\Delta\Delta G_{bind}$ is 6-fold less than the $\Delta\Delta G_{cat}$, which further indicates that the hydrogen bonds formed by Ser^{33} function predominantly in the catalytic step and not in the binding step. The $\Delta\Delta G_{b+c}$ of the $Ser^{33} \rightarrow Ala^{33}$ mutant is 1.6 kcal/mol. This value is similar to the experimental value of $\Delta\Delta G_T$ (1.1 kcal/mol) although the substrates for the $\Delta\Delta G_{b+c}$ and $\Delta\Delta G_T$ are different. As shown in Table 3, the mutants

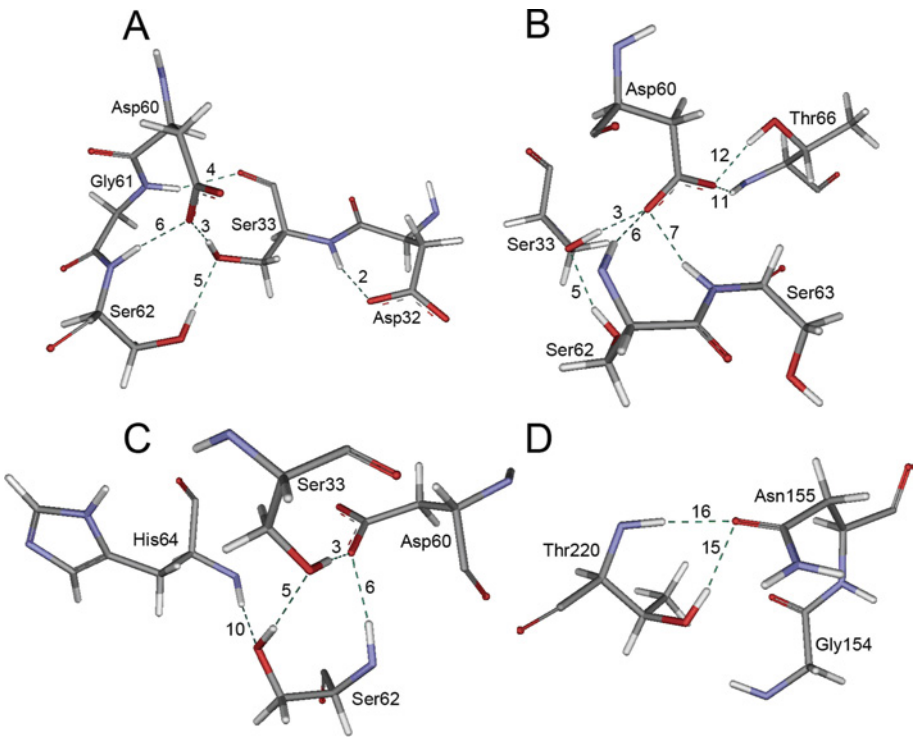

Figure 3 The hydrogen bonding interactions of Ser^{33}, Asp^{60}, Ser^{62} and Thr^{220} residues

(**A**) Hydrogen bond interactions of Ser^{33}. (**B**) Hydrogen bond interactions of Asp^{60}. (**C**) Hydrogen bond interactions of Ser^{62}. (**D**) Hydrogen bond interactions of Thr^{220}. The residues from NK are in standard atomic colours, labelled by residue name, and shown with the line rendering. This picture was created using Weblab Viewlite 5.0. Dashed lines are hydrogen bonds.

Table 3 Kinetic constants for the wild-type and mutant NK reactions with SUB1, and the results of three different types of FEP calculation

Another substrate, SUB2, was used in FEP calculations. -∞, the results of FEP calculations trend to negative infinity; NA, not available.

Enzyme	k_{cat} (s^{-1})	K_m (μM)	k_{cat}/K_m ($s^{-1} \cdot mM^{-1}$)	$\Delta\Delta G_T$ (kcal/mol)	ΔG_{solv} (kcal/mol)	ΔG_{bind} (kcal/mol)	ΔG_{cat} (kcal/mol)	$\Delta\Delta G_{bind}$ (kcal/mol)	$\Delta\Delta G_{cat}$ (kcal/mol)	$\Delta\Delta G_{b+c}$ (kcal/mol)
Wild-type	52.1	196	265.3	NA	NA	NA	NA	NA	NA	NA
Mutant										
S33A	16.5	358	46.1	1.1	7.1	7.4	8.7	0.3	1.3	1.6
D60A	3.7	527	7.0	2.2	-∞	-∞	-∞	NA	NA	NA
S62A	8.2	386	21.2	1.6	6.4	7.1	8.1	0.7	1.0	1.7
T220A	6.5	432	15.0	1.8	9.1	9.8	10.9	0.7	1.1	1.8

Ser^{62} → Ala^{62} and Thr^{220} → Ala^{220} have similar properties in this respect compared with the Ser^{33} → Ala^{33} mutant.

MD simulations

Based on the catalytic mechanism of subtilisin [7], the MD simulations focused on the structural alternations in the catalytic triad and the oxyanion hole of NK. Our investigation of the crystal structures of subtilisins with or without their proteinaceous inhibitors revealed a number of interesting findings about the catalytic triad. In all subtilisins, either with or without inhibitors, the $O_\delta1$(Asp^{32})–e1(His^{64}) distance is 3.0–3.2 Å, and the $O_\delta2$(Asp^{32})–e1(His^{64}) distance is 2.5–2.7 Å. These statistical data are in accordance with our MD results. As shown in Table 2, the HNe1(His^{64})–$O_\delta1$(Asp^{32}) distance remains approx. 1.8 Å, which is the distance trajectory of hydrogen bond-8, and the HNe1(His^{64})–$O_\delta2$(Asp^{32}) distance remains approx. 2.7 Å, which is the distance trajectory of hydrogen bond-9. With the aid of hydrogen bond-8 and hydrogen bond-9, the carboxyl terminal of Asp^{32} can act on HNe1(His^{64}) strengthening the negative charge on the imidazole of His^{64} [25]. Therefore it was clear that these two hydrogen bonds are strong and stable enough to exist in all three states and in the binding and catalytic steps.

In the crystal structures of subtilisins without inhibitors, the Ser^{221} residues can move freely. The Ne2(His^{64})–O_γ(Ser^{221}) distance remains approx. 2.5–4.0 Å. For example, the Ne2(His^{64})–O_γ(Ser^{221}) distance in the complex of subtilisin BPN′ with chymotrypsin inhibitor 2 M59k (PDB accession number 1LW6) is 2.64 Å, and that of the *Bacillus lentus* subtilisin (PDB 1C9J) is 3.93 Å. However, in these crystal structures of serine proteases with inhibitors, the Ser^{221} residue cannot move freely. The Ne2(His^{64})–O_γ(Ser^{221}) distance is restrained to 2.5–2.7 Å, which is the hydrogen bond distance. These statistical data suggest that substrates or inhibitors induce the inter-approach of Ne2(His^{64}) and HO_γ(Ser^{221}) in enzyme–substrate interactions. This inductive process is in accordance with the catalytic mechanism of Carter

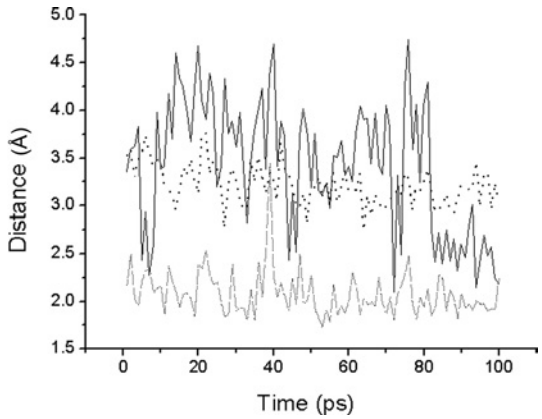

Figure 4 The distance trajectories for the native enzyme bound with substrate

The solid line is the distance between Ne2(His^{64}) and HO_{γ}(Thr^{220}). The dashed line is the distance between $HN_{\delta}2$(Asn^{155}) and O(Lys^{278}). The dotted line is the distance between O_{γ}(Ser^{221}) and C(Lys^{278}).

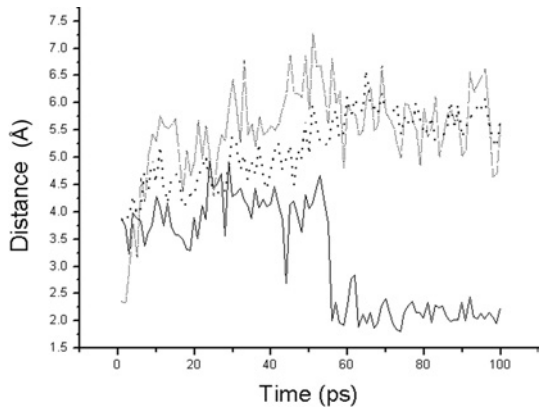

Figure 5 The distance trajectories for the Ser^{33} → Ala^{33} mutant bound with substrate

The solid line is the distance between Ne2(His^{64}) and HO_{γ}(Thr^{220}). The dashed line is the distance between $HN_{\delta}2$(Asn^{155}) and O(Lys^{278}). The dotted line is the distance between O_{γ}(Ser^{221}) and C(Lys^{278}).

and Wells [7]. Therefore the Michaelis complex structure that was modelled, which has a starting distance of 4.0 Å for Ne2(His^{64})–HO_{γ}(Ser^{221}), was chosen as our initial co-ordinate.

As shown in Figure 4, the 100 ps of MD simulation also supports the inductive interaction of substrates. As can be seen, the O_{γ}(Ser^{221})–C(Lys^{278}) distance gradually decreases from 3.6 to 3.0 Å during the 100 ps of MD simulation, which suggests that O_{γ}(Ser^{221}) is very stable and able to attack C(Lys^{278}). The hydrogen bond interaction between $HN_{\delta}2$(Asn^{155}) and O(Lys^{278}) is also stable at 2.0 Å during the 100 ps of MD simulation. The His^{64} residue; however, does not remain stable during the first 80 ps of MD simulation. The Ne2(His^{64})–O_{γ}(Ser^{221}) distance is increased by 2.5 to 4.5 Å, which is wider and stronger than that of the native enzyme without the bound substrate. After 80 ps, the Ne2(His^{64})–O_{γ}(Ser^{221}) distance is stable at 2.5 Å, which is the strong hydrogen bond distance. However, the interaction between Ne2(His^{64}) and O_{γ}(Ser^{221}) is weaker in the native enzyme without bound substrates and the distance gradually decreases from 4.0 to 3.0 Å during the 100 ps of MD simulation. We have therefore demonstrated that the substrate induces interaction between His^{64} and Ser^{221} residues when binding in the catalytic triad.

Effects of the hydrogen bonds from Ser^{33} on the catalytic efficiency of NK

Substituting Ala^{33} for Ser^{33} breaks hydrogen bond-3 and hydrogen bond-5 formed by the hydroxyl terminal of Ser^{33} as shown in Figure 3(A). The removal of these two hydrogen bonds directly results in decreasing catalytic efficiency of NK, which has been demonstrated by enzyme kinemics and FEP calculation as shown in Table 3. But why does catalytic efficiency decrease, and what effects does this have on the catalytic triad in the Ser^{33} → Ala^{33} mutant? During the 100 ps MD simulation without substrate, the Ne2(His^{64})–HO_{γ}(Ser^{221}) distance in the Ser^{33} → Ala^{33} mutant consistently remains approx. 4.0 Å. This distance trajectory does not trend to descend as in the native enzyme. It is evident that the Ala^{33} substitution does not contribute to the stability of Ser^{221} when there is no bound substrate. However, in the presence of a substrate, the Ne2(His^{64})–HO_{γ}(Ser^{221}) distance rapidly decreases from 4.0 to 2.0 Å after 50 ps, as shown in Figure 5. This suggests that the strong hydrogen bond interaction restrains the movement of Ser^{221}. However, the distances for $HN_{\delta}2$(Asn^{155})–O(Lys^{278}) and O_{γ}(Ser^{221})–C(Lys^{278}) increase to greater than 5.0 Å, which are both greater than the interaction distance. Therefore we concluded that the removal of hydrogen bond-3 and hydrogen bond-5 partially releases the Asp^{32} backbone atoms and allows Asp^{32} to move freely. When there is no substrate, Asp^{32} is found at the same starting co-ordinates as in the native enzyme. When the substrate is in complex with the enzyme, Asp^{32} moves closer to His^{64}, which increases the alkalinity of Ne2(His^{64}). At the same time, with the aid of the substrate's inductive interaction, the strong attraction of Ne2(His^{64}) for the hydroxyl group of Ser^{221} causes it to rapidly depart from the correct position for nucleophilic attack. Without the co-operation of O_{γ}(Ser^{221}), $HN_{\delta}2$(Asn^{155}) does not remain stable and dissociates from the substrate.

Threonine has the same function as serine at position 33. Comparing the sequence identity of the subtilisin family, we found that residue 33 is a conserved serine or threonine residue. Moreover, Thr^{33} can form the same hydrogen bonds as Ser^{33}, which are revealed in the crystal structure of subtilisin Carlsberg and subtilisin Savinase.

Effects of the Ser^{62} hydrogen bonds on the catalytic efficiency of NK

Substituting Ala^{62} for Ser^{62} breaks hydrogen bond-5 and hydrogen bond-10 formed by the hydroxyl group of Ser^{62} as shown in Figure 3(C). The removal of hydrogen bond-5 and hydrogen bond-10 partially releases the His^{64} backbone atoms. As a consequence, His^{64} can move freely. During the 100 ps MD simulation without substrate, the Ne2(H His^{64})–HO_{γ}(Ser^{221}) distance in the Ser^{62} → Ala^{62} mutant ranges between 2.0 and 4.5 Å. However, when the substrate is binding to enzyme, the unreleased residue Asp^{32} will restrain the movement of the His^{64} residue, even attracting it away from the correct position to interact with HO_{γ}(Ser^{221}). As shown in Figure 7, during the 100 ps MD simulation, the Ne2(His^{64})–HO_{γ}(Ser^{221}) distance remains approx. 4.0 Å, which is greater than the functional interaction distance. The O_{γ}(Ser^{221})–C(Lys^{278}) distance increases from 3.0 to 3.4 Å, which indicates that O_{γ}(Ser^{221}) is dissociating from C(Lys^{278}) during the 100 ps MD simulation. However the removal of hydrogen bond-5 and hydrogen bond-10 doesn't affect the stability of the oxyanion hole (Asn^{155}). The distance $HN_{\delta}2$(Asn^{155})–O(Lys^{278}) is consistently approx. 2.0 Å during the 100 ps MD simulation.

Similar to residue 33, residue 62 is either a conserved serine or aspartic acid residue. Thus Asn^{62} has the same role as Ser^{62} in subtilisins.

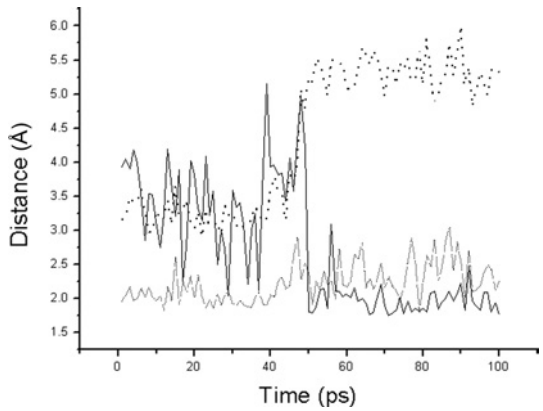

Figure 6 The distance trajectories for the Asp^{60} → Ala^{60} mutant bound with substrate

The solid line is the distance between Ne2(His^{64}) and HO_γ(Thr^{220}). The dashed line is the distance between $HN_\delta2$(Asn^{155}) and O(Lys^{278}). The dotted line is the distance between O_γ(Ser^{221}) and C(Lys^{278}).

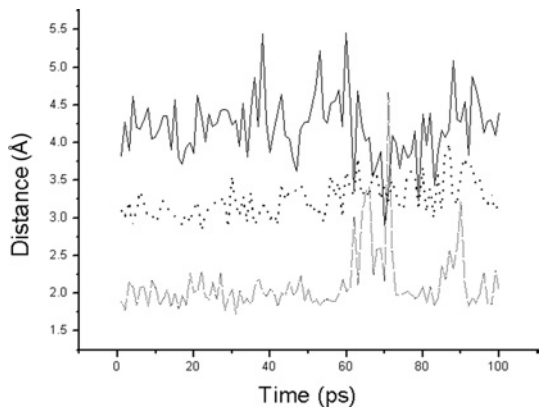

Figure 7 The distance trajectories for the Ser^{62} → Ala^{62} mutant bound with substrate

The solid line is the distance between Ne2(His^{64}) and HO_γ(Thr^{220}). The dashed line is the distance between $HN_\delta2$(Asn^{155}) and O(Lys^{278}). The dotted line is the distance between O_γ(Ser^{221}) and C(Lys^{278}).

Effects of the Asp^{60} hydrogen bonds on catalytic efficiency of NK

Substituting Ala^{60} for Asp^{60} breaks five hydrogen bonds (hydrogen bond-3, -6, -7, -11 and -13) formed by the carboxyl group of Asp^{60} as shown in Figure 3(B). The removal of these five hydrogen bonds releases the Asp^{32} and His^{64} backbone atoms, which is similar to mutating Ser^{33} and Ser^{62} at the same time. When there is no bound substrate, without the restraint of Asp^{32}, Ne2(His^{64}) rotates into close proximity to HO_γ(Ser^{221}) and moves around HO_γ(Ser^{221}) into a functional interaction distance. During the first 50 ps of MD simulation without substrate, the Ne2(His^{64})–HO_γ(Ser^{221}) distance of the Asp^{60} → Ala^{60} mutant gradually decreases from 4.0 to 3.0 Å, and then fluctuates between 2.0 and 3.5 Å after 50 ps. When the substrate is binding to the enzyme, the catalytic activity increases during the first 50 ps of MD simulation. As shown in Figure 6, the $HN_\delta2$(Asn^{155})–O(Lys^{278}) distance is stable at 2.0 Å, which is the functional hydrogen bond interaction distance. The O_γ(Ser^{221})–C(Lys^{278}) distance is also stable at 3.0 Å which is the functional interaction distance for nucleophilic attack. In addition, the Ne2(His^{64})–HO_γ(Ser^{221}) distance fluctuates between 2.0 and 5.0 Å as in the native enzyme. Therefore it was clear that the MD results during the first 50 ps are in accordance with the results of the FEP calculations shown in Table 3.

However, after 50 ps, the alkalinity of the imidazole of His^{64} is rapidly increased in the interaction with the released Asp^{32}, which strengthens the interaction between Ne2(His^{64}) and HO_γ(Ser^{221}). At the same time, with the help of the substrate's inductive interaction, Ne2(His^{64}) attracts the hydroxyl group of Ser^{221} to move away from the correct position for nucleophilic attack. As shown in Figure 6, the Ne2(His^{64})–HO_γ(Ser^{221}) distance decreases to 2.0 Å, and the O_γ(Ser^{221})–C(Lys^{278}) distance rapidly increases to 5.5 Å. As shown, the catalytic activity rapidly decreases after a 50 ps MD simulation.

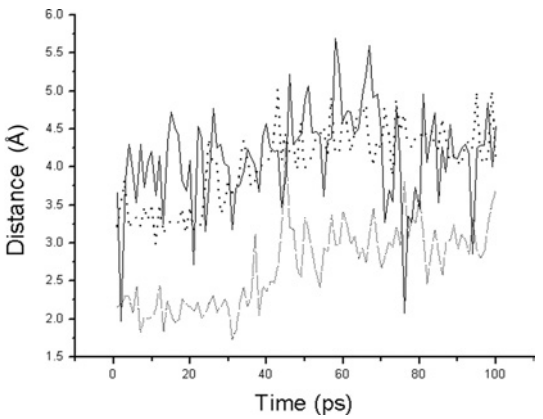

Figure 8 The distance trajectories for the Thr^{220} → Ala^{220} mutant bound with substrate

The solid line is the distance between Ne2(His^{64}) and HO_γ(Thr^{220}). The dashed line is the distance between $HN_\delta2$(Asn^{155}) and O(Lys^{278}). The dotted line is the distance between O_γ(Ser^{221}) and C(Lys^{278}).

Effects of the Thr^{220} hydrogen bonds on catalytic efficiency of NK

Substituting Ala^{220} for Thr^{220} breaks hydrogen bond-15 formed by the hydroxyl group of Thr^{220} as shown in Figure 3(D). As shown, the stability of Asn^{155} relies on two hydrogen bonds, hydrogen bond-15 and hydrogen bond-16. The removal of hydrogen bond-15 partially releases the Asn^{155} residue, and forces $HN_\delta2$(Asn^{155}) to move freely [22]. As shown in Figure 8, the $HN_\delta2$(Asn^{155})–O(Lys^{278}) distance gradually decreases from 2.0 to 3.0 Å during the 100 ps MD simulation [21]. The instability of $HN_\delta2$(Asn^{155}) directly results in the instability of O_γ(Ser^{221}). The O_γ(Ser^{221})–C(Lys^{278}) distance increases to 4.5 Å, as shown in Figure 8. However, the instability of $HN_\delta2$(Asn^{155}) doesn't affect the interaction between Ne2(His^{64}) and HO_γ(Ser^{221}). The Ne2(His^{64})–HO_γ(Ser^{221}) distance always increases from 2.0 to 4.5 Å as in the native enzyme.

Braxton and Wells [21] have demonstrated that the stabilizing effects of Thr^{220} are mediated either via a short-range charedipolar interaction or by dynamic fluctuations in the protein structure, which permits direct hydrogen bonding with oxyanion. The results calculated by Mizushima et al. [22] further demonstrated that -OH(Thr^{220}) is important for catalysis but not to as great an extent as a hydrogen-bonding group, such as Asn^{155}, positioned directly in the oxyanion hole.

This work was mostly supported by the National Natural Scientific Foundation (grant numbers 30370366 and 30470111) and supported in part by a grant (number 92-2313-B-007-002) from the NSC (National Science Council Taiwan). The AMBER studies were conducted at the National Centre for High Performance Computing, Taiwan. We are grateful to Dr Keng-chang Tsai for his fruitful discussions concerning the results of enzyme kinetics and MD simulation.

REFERENCES

1 Sumi, H. (1987) A novel fibrinolytic enzyme in the vegetable cheese natto: a typical and popular soybean food in the Japanese diet. Experientia **43**, 1110–1111
2 Jovin, I. S. and Müller, B. G. (2004) Inter-relationships between the fibrinolytic system and lipoproteins in the pathogenesis of coronary atherosclerosis. Atherosclerosis **174**, 225–233
3 Ko, J. H., Yan, J. P., Zhu, L. and Qi, Y. P. (2004) Identification of two novel fibrinolytic enzymes from *Bacillus subtilis* QK02. Comp. Biochem. Physiol. **137**, 65–74
4 Bryan, P. N. (2000) Protein engineering of subtilisin. Biochim. Biophys. Acta **1543**, 203–222
5 Takagi, H., Koga, M., Katsurada, S., Yabuta, Y., Shinde, U. and Inouye, M. (2001) Functional analysis of the propeptides of subtilisin E and aqualysin I as intramolecular chaperones. FEBS Lett. **508**, 210–214
6 Yang, Y. H., Jiang, L., Zhu, L. Q., Wu, Y. J. and Yang, S. L. (2000) Thermal stable and oxidation-resistant variant of subtilisin E. J. Biotech. **81**, 113–118
7 Carter, P. and Wells, J. A. (1988) Dissecting the catalytic triad of a serine protease. Nature (London) **332**, 564–568
8 Baker, D. and Sali, A. (2001) Protein structure, prediction and structural genomics. Science (Washington, DC) **294**, 93–96
9 Skolnick, J. and Fetrow, J. S. (2000) From genes to protein structure and function: novel applications of computational approaches in the genomic era. Trends Biotechnol. **18**, 34–39
10 Higuchi, R., Krummel, B. and Saiki, R. K. (1988) A general method of *in vitro* preparation and specific mutagenesis of DNA fragments: study of protein and DNA interactions. Nucleic Acids Res **16**, 7351–7367
11 Ho, S. N., Hunt, H. D., Horton, R. M., Pullen, J. K. and Pease, L. R. (1989) Site-directed mutagenesis by overlap extension using the polymerase chain reaction. Gene **77**, 51–59
12 Brow, M. A. D. (1990) Sequencing with *Taq* DNA polymerase. In PCR protocols: A guide to Methods and Applications (Innis, M. A., Gelfand, D. H., Sninsky, J. J. and White, T. J., eds.), pp. 189–196, Academic Press, San Diego, CA, U.S.A.
13 Innis, M. A., Myambo, K. B., Gelfand, D. H. and Brow, M. A. (1988) DNA sequencing with *Thermus aquaticus* DNA polymerase and direct sequencing of polymerase chain reaction-amplified DNA. Proc. Natl. Acad. Sci. U.S.A. **85**, 9436–9440
14 Peng, Y., Huang, Q., Zhang, R. H. and Zhang, Y. Z. (2003) Purification and characterization of a fibrinolytic enzyme produced by *Bacillus amyloliquefaciens* DC-4 screened from *douchi*, a traditional Chinese soybean food. Comp. Biochem. Physiol. **134**, 45–52
15 Astrup, T. and Mullertz, S. (1952) The fibrin plate method for estimating fibrinolytic activity. Arch. Biochem. Biophys. **40**, 346–351
16 Zheng, Z. L., Zou, G. L., Liu, Z. G., Tsai, K. C., Lie, A. F. and Zou, G. L. (2005) Construction of a 3D model of nattokinase, a novel fibrinolytic enzyme from *Bacillus natto*. A novel nucleophilic catalytic mechanism for nattokinase. J. Mol. Graph. Mod. **23**, 373–380
17 Prokop, M., Damborsky, J. and Koca, J. (2000) TRITON: *in silico* construction of protein mutants and prediction of their activities. Bioinformatics **16**, 845–846
18 Damborsky, J., Prokop, M. and Koca, J. (2001) TRITON: graphic software for rational engineering of enzymes. Trends Biochem. Sci. **26**, 71–73
19 Van Gunsteren, W. F. and Berendsen, H. J. C. (1977) Algorithms for macromolecular dynamics and constraint dynamics. Mol. Phys. **34**, 1311–1327
20 Pearlman, D. A. and Kollman, P. A. (1989) A new method for carrying out free energy perturbation calculation: dynamically modified windows. J. Chem. Phys. **90**, 2460–2470
21 Braxton, S. and Wells, J. A. (1991) The importance of a distal hydrogen bonding group in stabilizing the transition state in subtilisin BPN′. J. Biol. Chem. **266**, 11797–11800
22 Mizushima, N., Hirono, S., Pearlman, D. and Kollman, P. A. (1991) Free energy perturbation calculation on binding and catalysis after mutating threonine 220 in subtilisin. J. Biol. Chem. **18**, 11801–11809
23 Ballinger, M. D., Tom, J. and Wells, J. A. (1995) Designing subtilisin BPN′ to cleave substrates containing dibasic residues. Biochemistry **34**, 13312–13319
24 Fujita, M., Nomura, K., Hong, K., Ito, Y., Asada, A. and Nishimuro, S. (1993) Purification and characterization of a strong fibrinolytic enzyme (Nattokinase) in the vegetable cheese Natto, a popular soybean fermented food in Japan. Biochem. Biophys. Res. Commun. **30**, 1340–1347
25 Thomas, P. G., Russell, A. J. and Fersht, A. R. (1985) Tailoring the pH dependence of enzyme catalysis using protein engineering. Nature (London) **318**, 375–376

Received 11 May 2005/13 January 2006; accepted 17 January 2006
Published as BJ Immediate Publication 17 January 2006, doi:10.1042/BJ20050772